

Article

Ferroelectric and Spectroscopic Properties of Ho³⁺/Yb³⁺ Co-Doped Pb(Mg_{1/3}Nb_{2/3})O₃-32PbTiO₃ Crystal

Jin Zhang ¹, Zengzhe Xi ^{1,2,*}, Xinzhe Wang ², Shenghan Gao ³, Xinyi Long ² and Feifei Guo ¹

¹ School of Materials and Chemical Engineering, Xi'an Technological University, Xi'an 710021, China; zhangj@xatu.edu.cn (J.Z.); guoifeifei19850106@outlook.com (F.G.)

² Shaanxi Key Laboratory of Photoelectric Functional Materials and Devices, Xi'an 710021, China; owlwithleaves@outlook.com (X.W.); longxy1998@outlook.com (X.L.)

³ School of Queen Mary, Nanchang University, Nanchang 330031, China; jp4217120242@qmul.ac.uk

* Correspondence: zzhxi@xatu.edu.cn; Tel.: +86-29-86173324

Abstract: In order to design a new multifunctional crystal with excellent ferroelectric and spectroscopic properties, experiments were carried out for Ho³⁺/Yb³⁺ co-doped Pb(Mg_{1/3}Nb_{2/3})O₃-32PbTiO₃ ferroelectric crystal using the flux method, the coercive field E_c of which is 11.86 kV/cm. Up-conversion luminescence emission bands, including an intense green emission band at 553 nm, a red band at 663 nm, and a weak infra-red band at 755 nm, are generated at 980 nm excitation. The main spectroscopic parameters, including radiative transition probability $A(J' - J)$, radiative lifetimes τ_{rad} , and branching ratios β , were predicted by applying Judd–Ofelt treatment. The obtained J-O intensity parameters are $\Omega_2 = 0.531 \times 10^{-20} \text{ cm}^2$, $\Omega_4 = 1.738 \times 10^{-20} \text{ cm}^2$, $\Omega_6 = 0.530 \times 10^{-20} \text{ cm}^2$. The radiative lifetime of ⁵I₇ level is 5.45 ms. The fluorescence lifetime of is ⁵F₅ is 92.568 μ s. The investigations show that Ho³⁺/Yb³⁺ co-doped Pb(Mg_{1/3}Nb_{2/3})O₃-0.32PbTiO₃ crystal is a new type of multifunctional crystal integrating ferroelectric and spectroscopic properties, which has a potential application in the developing innovative multifunctional devices and lasers.



Citation: Zhang, J.; Xi, Z.; Wang, X.; Gao, S.; Long, X.; Guo, F. Ferroelectric and Spectroscopic Properties of Ho³⁺/Yb³⁺ Co-Doped Pb(Mg_{1/3}Nb_{2/3})O₃-32PbTiO₃ Crystal. *Crystals* **2022**, *12*, 225. <https://doi.org/10.3390/cryst12020225>

Academic Editors: Peter Baran and Shujun Zhang

Received: 16 January 2022

Accepted: 2 February 2022

Published: 4 February 2022

Publisher's Note: MDPI stays neutral with regard to jurisdictional claims in published maps and institutional affiliations.



Copyright: © 2022 by the authors. Licensee MDPI, Basel, Switzerland. This article is an open access article distributed under the terms and conditions of the Creative Commons Attribution (CC BY) license (<https://creativecommons.org/licenses/by/4.0/>).

Keywords: Judd–Ofelt; PMN-32PT; Er³⁺; ferroelectric; crystal; spectroscopic

1. Introduction

In recent decades, relaxor ferroelectric single crystals represented by (1-x) Pb(Mg_{1/3}Nb_{2/3})O₃-xPbTiO₃ [PMN-PT] and Pb(Zn_{1/3}Nb_{2/3})O₃-xPbTiO₃ [PZN-PT] have triggered a revolution. They are regarded as potential materials in the medical ultrasonic probe, underwater acoustic transducer, and ultrasonic motor owing to their excellent electric properties [1–3]. However, the low coercive field E_c limits their applications in high-power devices. It is urgent to develop a new-type ferroelectric single crystal with high coercive field E_c .

In addition, PMN-PT and PZN-PT relaxor ferroelectric crystals do not contain luminescent activators, which limits their application in optical devices and opto-electric couplers. Rare earth (RE) ions (Er³⁺, Ho³⁺, Eu³⁺, Tb³⁺, Tm³⁺, and Sm³⁺), as well-known activators with optical emission in the infrared and visible wavelength ranges, have been widely doped into the host material to design luminescent materials. In addition, RE ions are used in the electricity fields owing to their unique chemical properties. Therefore, new ferroelectric crystals doped with RE ions, such as Pb(Sm_{1/2}Nb_{1/2})O₃-Pb(Mn_{1/3}Nb_{2/3})O₃-PbTiO₃ [4], Sm doped Pb(Mn_{1/3}Nb_{2/3})O₃-PbTiO₃ [5], Ho³⁺ doped PZN-PT [6], Pb(Sc_{1/2}Nb_{1/2})O₃-Pb(Mn_{1/3}Nb_{2/3})O₃-PbTiO₃ doping with Ho³⁺ and Ho³⁺/Yb³⁺ [7], and Pb(Ho_{1/2}Nb_{1/2})O₃-Pb(Mn_{1/3}Nb_{2/3})O₃-PbTiO₃ [8], have successfully grown in the last five years. Rare earth ions as solid solutions and impurity ions enter PMN-PT and PZN-PT crystals.

Investigations have shown that some new-type ferroelectric crystals have higher coercive field E_c . It was reported that the coercive field E_c of Ho³⁺/Yb³⁺ co-doped PZN-PT crystal is about 9.26 kV/cm [9], which is higher than that of PZN-PT:Ho³⁺ ($E_c \sim 5.9$ kV/cm) [6]

and $\text{Pb}(\text{Sm}_{1/2}\text{Nb}_{1/2})\text{O}_3\text{-Pb}(\text{Zn}_{1/3}\text{Nb}_{2/3})\text{O}_3\text{-PbTiO}_3$ ($E_c \sim 3.61$ kV/cm) [4] crystals. In addition, some new-type ferroelectric crystals own excellent luminescence properties. It was reported that an intense green emission band at 552 nm were observed in Ho^{3+} and $\text{Ho}^{3+}/\text{Yb}^{3+}$ co-doped $\text{Pb}(\text{Sc}_{1/2}\text{Nb}_{1/2})\text{O}_3\text{-Pb}(\text{Zn}_{1/3}\text{Nb}_{2/3})\text{O}_3\text{-PbTiO}_3$ by 980 nm laser excitation. The emission intensity of $\text{Ho}^{3+}/\text{Yb}^{3+}$ co-doped $\text{Pb}(\text{Sc}_{1/2}\text{Nb}_{1/2})\text{O}_3\text{-Pb}(\text{Zn}_{1/3}\text{Nb}_{2/3})\text{O}_3\text{-PbTiO}_3$ was increased by three orders of magnitude compared to the single doping of Ho^{3+} ions. In this case, the Yb^{3+} , as an optical sensitive ion, enhances the luminescence intensity [7].

In order to provide an understanding of the spectroscopic properties of the new-type ferroelectric crystals doped with rare earth ions, it is necessary to apply Judd–Ofelt treatment on them. The main spectroscopic characteristics, including radiative transition probability, radiative lifetimes, branching ratios, and emission cross section, can be obtained by applying Judd–Ofelt theory. Judd–Ofelt treatment is widely applied to predict the spectroscopic characteristics for laser crystals [10–19]. However, relevant Judd–Ofelt treatment on the new-type ferroelectric crystals doping with rare earth ions could not be found in the previous literature.

In this work, $\text{Ho}^{3+}/\text{Yb}^{3+}$ were doped into PMN-32PT ferroelectric single crystals to form a new system. Judd–Ofelt treatment is performed on the PMN-32PT: $\text{Ho}^{3+}/\text{Yb}^{3+}$ ferroelectric crystal for the first time. Oscillator and spectral strength parameters, including Judd–Ofelt parameters Ω_t ($t = 2, 4, \text{ and } 6$), radiative transition probabilities $A(J' - J)$, branching ratio β , and radiative lifetime τ_{rad} , were predicted. This investigation will provide a theoretical basis for the luminescence mechanism. In addition, the effect of $\text{Ho}^{3+}/\text{Yb}^{3+}$ ions on the ferroelectric properties of PMN-32PT crystal has been studied. Our research is as follows: Firstly, the experiments were carried out for $\text{Ho}^{3+}/\text{Yb}^{3+}$ co-doped $\text{Pb}(\text{Mg}_{1/3}\text{Nb}_{2/3})\text{O}_3\text{-32PbTiO}_3$ ferroelectric crystal using the flux method. Secondly, the main characteristics, including XRD, EDS, hysteresis loops, absorption, and up-conversion luminescence emission spectra of the crystals, were investigated. Finally, the spectroscopic parameters of PMN-32PT: $\text{Ho}^{3+}/\text{Yb}^{3+}$ crystal were predicted by applying the Judd–Ofelt treatment.

2. Materials and Methods

2.1. Crystal Growth

PMN-32PT: $\text{Ho}^{3+}/\text{Yb}^{3+}$ crystal was grown by the high-temperature flux method. The process is shown in Figure 1:

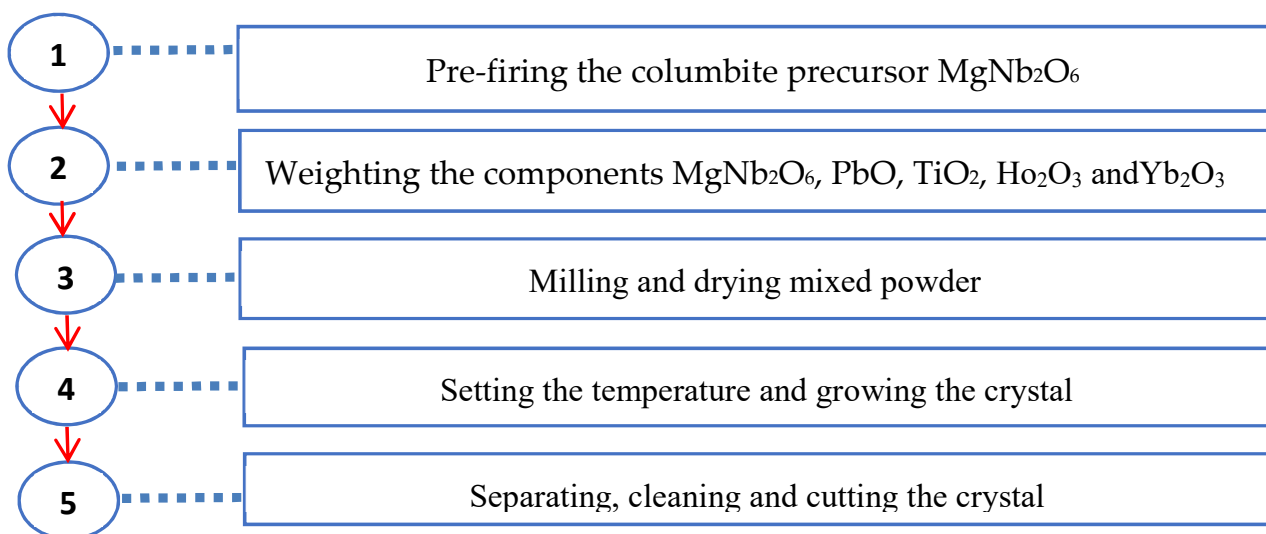


Figure 1. The steps of PMN-32PT: $\text{Ho}^{3+}/\text{Yb}^{3+}$ crystal growth.

Step 1: PbO, MgO, Nb₂O₅, Ho₂O₃, Yb₂O₃, and TiO₂ powders with 99.99% purity were used as starting materials. MgO and Nb₂O₅ powders were mixed at a molar ratio of 1:1 and calcinated at 1000 °C for 6 h to form the precursor MgNb₂O₆.

Step 2: MgNb₂O₆, PbO, and TiO₂ powders were mixed according to the stoichiometric composition 0.68PMN–0.32PT. Meanwhile, the 2 mol% Ho₂O₃ and Yb₂O₃, together with excessive 80 wt% PbO powders, were also added to the mixtures.

Step 3: The mixtures were wet-milled for 12 h in the alcohol and dried at 80 °C for 24 h in a drying oven. Then, the dried mixture powders were poured into a platinum crucible which was placed in a corundum pot.

Step 4: The crucibles were placed in the crystal growth furnace with an automatic temperature controller, which was set from room temperature to 1330 °C at the rate of 3 °C/min, held for 12 h, and fell from 1330 °C to 650 °C at the rate of 0.01 °C/min, then cooled to room temperature spontaneously. Two weeks later, the as-grown PMN-32PT:Ho³⁺/Yb³⁺ crystals were obtained.

Step 5: The as-grown single crystals PMN-32PT:Ho³⁺/Yb³⁺ together with Pt crucible were boiled in nitric acid solution until the crystals were separated from the crucible. Then, PMN-32PT:Ho³⁺/Yb³⁺ crystal was cut into thin slices along the exposed surface. Finally, the silver paste was daubed on two sides as the electrodes and annealed at 550 °C for 2 h before testing ferroelectric properties.

2.2. Characterization Procedure

The X-ray diffraction data was collected by X-Ray Diffractometer (Bruker D8 ADVANCE, Germany) with Cu K α radiation. Energy dispersive system (EDS) spectrum was obtained by a scanning electron microscope (Gemini SEM 500). The ferroelectric hysteresis loops were measured by aix-ACCT TF2000 analyzer. The absorption spectra were detected by UV-VIS-NIR spectrophotometer (UV3600PLUS, HIMADZU, JAPAN). The luminescence spectrum and the fluorescence lifetime were measured by Steady-State Spectrometer (FLS980, Edinburgh, England).

3. Results and Discussion

3.1. XRD Patterns

Figure 2 shows the XRD patterns of Ho³⁺/Yb³⁺ co-doped PMN-32PT crystal powders together with undoped PMN-32PT for comparison. One can see that the diffraction peaks of PMN-32PT:Ho³⁺/Yb³⁺ are consistent with PMN-32PT crystal. They are both pure perovskite structure (ABO₃) without any other phase. The enlarged view of (111) and (200) peaks is shown in Figure 2b,c. It can be seen that (111) and (200) peaks occur splitting, which indicates that Ho³⁺/Yb³⁺ diffuse into the PMN-32PT crystal lattices and induces the transition from rhombohedral phase into the tetragonal and rhombohedral phase. The tetragonal and rhombohedral phase coexist in the PMN-32PT:Ho³⁺/Yb³⁺ crystal.

3.2. EDS Spectrum

Figure 3a shows energy dispersive system (EDS) of three random points on the surface of PMN-32PT:Ho³⁺/Yb³⁺ crystals. The EDS spectrums of the three points are presented in Figure 3b–d. It can be seen from the figures that the chemical composition of the single crystal is Pb, Mg, Nb, Ti, and O. In addition, the Ho and Yb are also found, which indicates that Ho³⁺ and Yb³⁺ ions diffuse into single crystals. The element content of the crystals obtained by EDS is shown in Table 1. It is noticed that the element distribution of the crystal is homogeneity. According to the tested niobium and titanium content, the calculated chemical composition is close to the PMN-32PT. The weight content of Ho³⁺ and Yb³⁺ is about 1.62 wt% and 1.52 wt%, respectively.

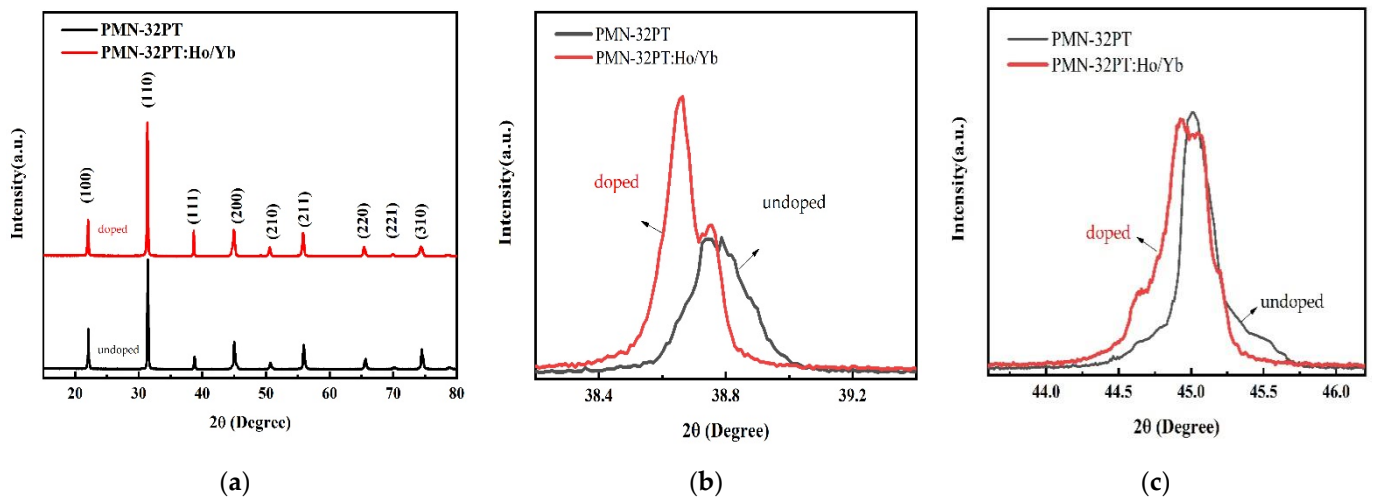


Figure 2. (a) XRD patterns from 10° to 80° of PMN-32PT:Ho³⁺/Yb³⁺ and PMN-PT crystal powders (b) enlarged XRD patterns from 38.2° to 39.5° (c) enlarged XRD patterns from 43.2° to 46.2° .

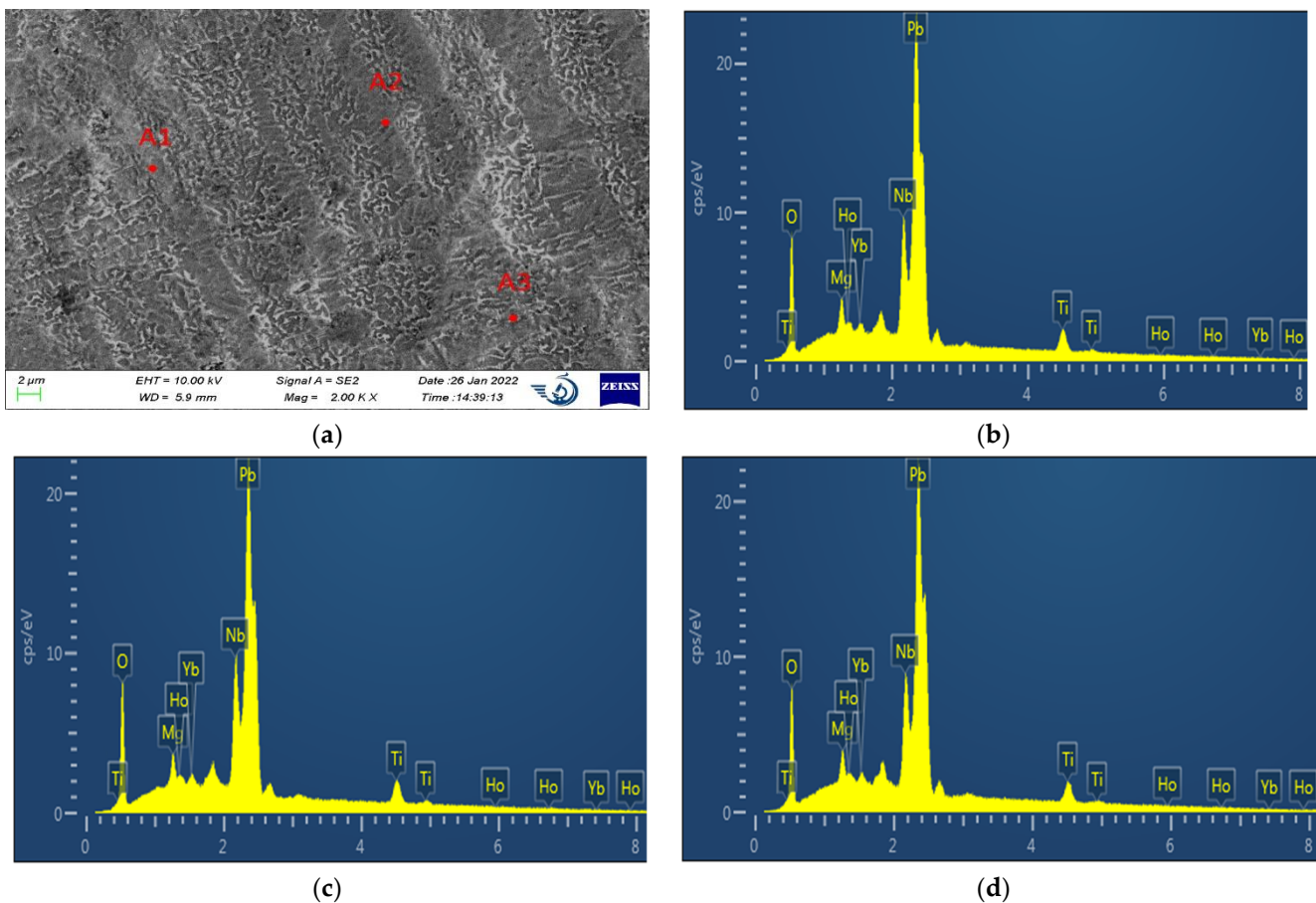


Figure 3. (a) energy dispersive system (EDS) of three random points on the surface of PMN-32PT:Ho³⁺/Yb³⁺ crystals. (b) EDS spectrum of A1. (c) EDS spectrum of A2. (d) EDS spectrum of A3.

Table 1. The element content of the PMN-32PT: Ho³⁺/Yb³⁺ crystals obtained by EDS.

	O	Pb	Mg	Ti	Nb	Ho	Yb
A1 (wt%)	6.49	68.76	1.19	5.59	14.82	1.59	1.55
A2 (wt%)	6.61	68.75	1.14	5.57	14.86	1.59	1.47
A3 (wt%)	6.77	66.00	1.07	6.25	16.69	1.68	1.54

3.3. Hysteresis Loops

Figure 4a shows the ferroelectric hysteresis loop of Ho³⁺/Yb³⁺ doped PMN-32PT single crystal. It can be seen from the figure that the hysteresis loop of PMN-32PT: Ho³⁺/Yb³⁺ single crystal gradually becomes saturation when the external electric field was increased from 4 kV/cm to 16 kV/cm. The spontaneous polarization (P_s) and residual polarization (P_r) of Ho³⁺/Yb³⁺ doped PMN-32PT crystal is 22.52 $\mu\text{C}/\text{cm}^2$ and 20.85 $\mu\text{C}/\text{cm}^2$, respectively, which is similar with that of undoped PMN-PT crystals ($P_s \sim 23.29 \mu\text{C}/\text{cm}^2$, $P_r \sim 19.38 \mu\text{C}/\text{cm}^2$) shown in Figure 4b. However, the coercive field ($E_c \sim 11.86 \text{ kV}/\text{cm}$) of PMN-32PT:Ho³⁺/Yb³⁺ crystal is higher than that of undoped PMN-PT crystals ($E_c \sim 3.92 \text{ kV}/\text{cm}$). The enhancement in coercive field in the crystals could be attributed to the distorted lattice and oxygen vacancy to pin the domain wall motion [7,8]. As the radius of doping ions Ho³⁺ (0.089 nm) and Yb³⁺ (0.086 nm) are close to that of the cations (Mg²⁺: $r \sim 0.072 \text{ nm}$; Nb⁵⁺: $r \sim 0.064 \text{ nm}$; and Ti⁴⁺: $r \sim 0.0605 \text{ nm}$) located the B-site, Ho³⁺ and Yb³⁺ ions preferentially occupy the B-site and distort the crystal lattice (demonstrated in XRD results). Large lattice distortion induces high stress, which limits the domain switching, resulting in the E_c increase. On the other hand, considering the different valence states among Ho³⁺, Yb³⁺, Mg²⁺, Nb⁵⁺, and Ti⁴⁺, some charged ions such as oxygen vacancies will be formed for compensating charge balance. The combination of doped cations (Er³⁺ or Yb³⁺) and oxygen vacancies form defect dipoles. The defect dipole is consistent with each other in the short range, which act as pinning points to prevent the domain moving. Therefore, the coercive field was enhanced.

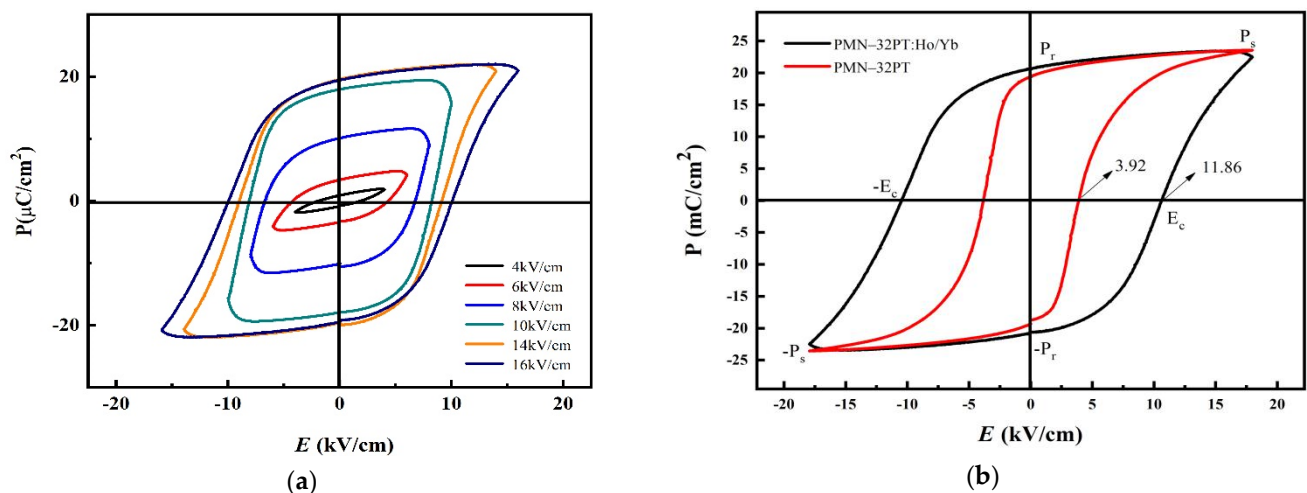


Figure 4. (a) Polarization versus electric field (P - E) hysteresis loops with different electric fields (b) P - E hysteresis loops of the crystals PMN-32PT:Ho³⁺/Yb³⁺ and PMN-32PT at saturated state.

3.4. UV-VIS-NIR Absorption

Figure 5 shows the absorption spectra of the PMN-32PT:Ho³⁺/Yb³⁺ single crystal at 300 K. Seven absorption peaks were observed in the range of 450 nm–2200 nm. The peaks located at 451 nm, 541 nm, 643 nm, 1152 nm, and 1943 nm correspond to the transitions $^5G_6/^5F_1 \rightarrow ^5I_8$ (451 nm), $^5F_4/^5S_2 \rightarrow ^5I_8$ (541 nm), $^5F_5 \rightarrow ^5I_8$ (643 nm), $^5I_6 \rightarrow ^5I_8$ (1152 nm), and $^5I_7 \rightarrow ^5I_8$ (1943 nm) of Ho³⁺ ions, respectively. The peaks at 902 nm and 974 nm correspond to the transition absorption of Yb³⁺ ions. The special line at 800–860 nm is caused by the

switching from infrared detectors to visible light detectors. The obtained absorption spectra of PMN-32PT:Ho³⁺/Yb³⁺ single crystal is very similar to that of PSN-PMN-PT:Ho³⁺/Yb³⁺ crystal [7], which have similar structure. The number of observed absorption peaks is limited by the energy band gap of the host crystals. Hence, only five absorption bands of Ho³⁺ in the spectrum are explored. It is less than that of laser crystals LiNbO₃:In³⁺/Ho³⁺ [11], YAlO₃:Ho³⁺ [12], YAG:Ho³⁺ [13], and Gd₃(Al,Ga)₅O₁₂:Ho³⁺/Yb³⁺ [14]. It seems that it is necessary to apply the Judd–Ofelt treatment to analyze the absorption spectrum shown in Figure 5.

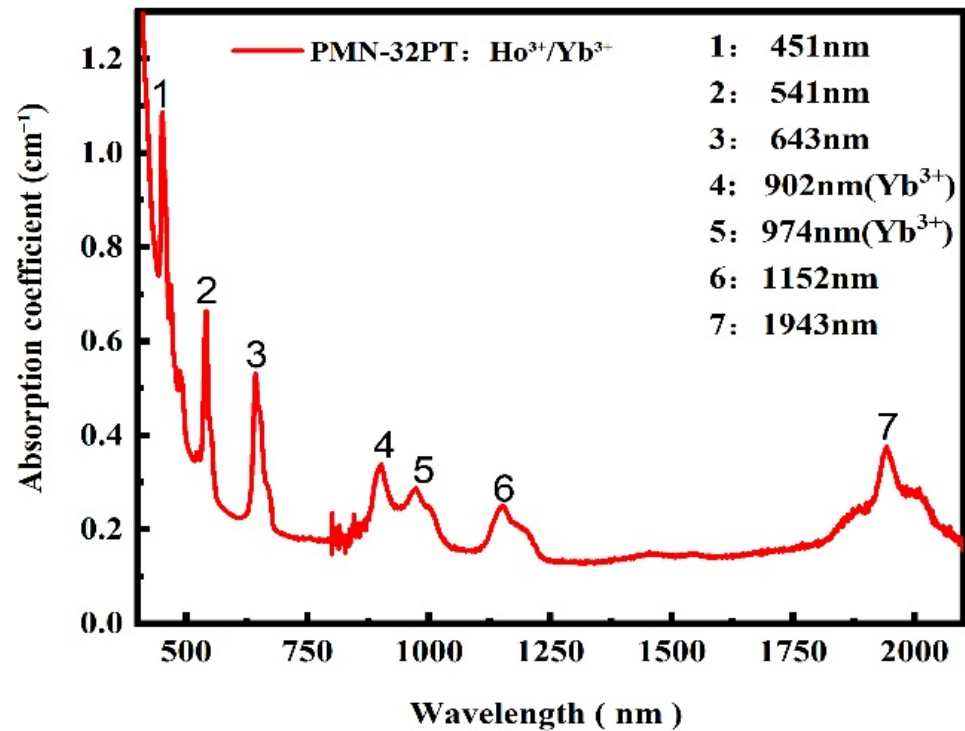


Figure 5. The absorption spectra of PMN-32PT:Ho³⁺/Yb³⁺ crystals.

3.5. Judd–Ofelt Analysis

Figure 6 shows the main steps of Judd–Ofelt treatment on the PMN-PT:Ho³⁺/Yb³⁺ crystal:

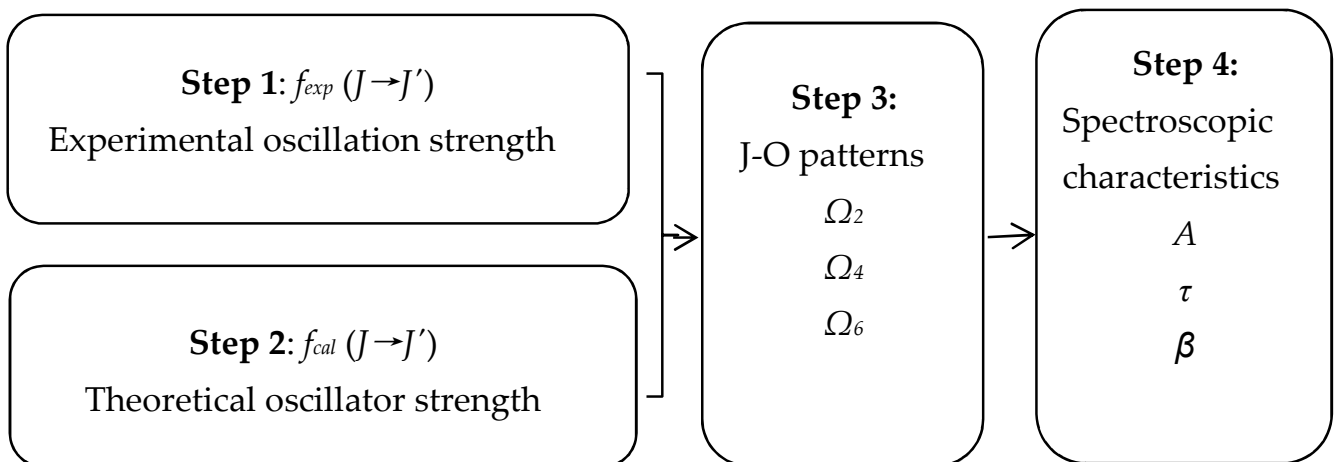


Figure 6. The main steps of Judd–Ofelt treatment on PMN-32PT: Ho³⁺/Yb³⁺.

Step 1: The experimental oscillation strength, $f_{exp}(J \rightarrow J')$, of Ho^{3+} in the PMN-32PT crystal are obtained by Equation (1). There are only five optical absorption bands from the ground state 5I_8 of Ho^{3+} ions in the spectrum shown in Figure 5. The experimental oscillation strength $f_{exp}(J \rightarrow J')$ of these five bands are obtained from analysis of the five integral absorption coefficients $\int \alpha(\lambda) d\lambda$.

$$f_{exp}(J \rightarrow J') = \frac{mc^2}{\pi e^2 \bar{\lambda}^2 N_0} \int \alpha(\lambda) d\lambda \quad (1)$$

where J is the ground state 5I_8 , J' is the excited state, c is the speed of light in vacuum, m and e are the electron mass and charge, respectively, and N_0 is the holmium concentration. In this paper, $\bar{\lambda}$ is the average wavelength of the $J \rightarrow J'$ transition. $\alpha(\lambda)$ is absorption coefficient, which obtained from absorption spectra testing.

Step 2: The theoretical oscillator strength, $f_{cal}(J \rightarrow J')$, of Ho^{3+} in the PMN-PT crystal is given by Equation (2):

$$f_{cal}(J \rightarrow J') = \frac{8\pi^2 mc}{3h(2J+1)n^2 \bar{\lambda}} (\chi_{ed} S_{ed} + \chi_{md} S_{md}) \quad (2)$$

where h is the Planck constant and n is the refractive index of the host. $n = (2n_o + n_e)/3$ for crystals. The values of $n_o(\lambda)$ and $n_e(\lambda)$ used here for PMN-PT were derived from reference [15]. χ_{ed} and χ_{md} are the refractive index factors of electric dipole transition and magnetic dipole transition, respectively; they are given by Equations (3) and (4). S_{ed} and S_{md} are the line strengths for the electric dipole and magnetic dipole transitions, respectively. They are given by Equations (5) and (7).

$$\chi_{ed} = \frac{n(n^2 + 2)^2}{9} \quad (3)$$

$$\chi_{md} = n^3 \quad (4)$$

$$S_{md}(J \rightarrow J') = (h/4\pi mc)^2 \left| \left\langle 4f^N (SL)J \| L + 2S \| 4f^N (S'L')J' \right\rangle \right|^2 \quad (5)$$

$$\text{Selection rule of } S_{md} \text{ transitions : } \Delta l = 0; \Delta S = 0; \Delta L = 0; \Delta J = 0, \pm 1; \Delta M = 0, \pm 1 \quad (6)$$

$$S_{ed}(J \rightarrow J') = \sum_{t=2,4,6} \Omega_t \left| \left\langle 4f^N (SL)J \left\| U^{(t)} \right\| 4f^N (S'L')J' \right\rangle \right|^2 \quad (7)$$

$$\text{Selection rule of } S_{ed} \text{ transitions : } \Delta l = \pm 1; \Delta S = 0; |\Delta L| \leq 6; |\Delta J| \leq 6; \quad (8)$$

where the reduced matrix elements of the unit tensor operator, $U^{(t)}$ ($t = 2, 4$, and 6), are almost insensitive to the ion environment. The values used here were derived from reference [13]. In addition, $(L + 2S)$ is the magnetic dipole operator which depends on ΔJ :

$$J' = J \rightarrow \left| \left\langle 4f^N (SL)J \| L + 2S \| 4f^N ((S'L')J') \right\rangle \right| = \left[\frac{2J+1}{4J(J+1)} \right]^{1/2} \times [S(S+1) - L(L+1) + 3J(J+1)] \quad (9)$$

$$J' = J - 1 \rightarrow \left| \left\langle 4f^N (SL)J \| L + 2S \| 4f^N ((S'L')J') \right\rangle \right| = \left[\frac{((S+L+1)^2 - J^2)(J^2 - (L-S)^2)}{4J} \right]^{1/2} \quad (10)$$

$$J' = J + 1 \rightarrow \left| \left\langle 4f^N (SL)J \| L + 2S \| 4f^N ((S'L')J') \right\rangle \right| = \left[\frac{((S+L+1)^2 - (J+1)^2)((J+1)^2 - (L-S)^2)}{4(J+1)} \right]^{1/2} \quad (11)$$

Step 3: The J-O intensity parameters, Ω_t ($t = 2, 4$, and 6), are found by least-squares fitting the measured experimental oscillation strength (f_{exp}) values given by Formula (1) to the calculated theoretical ones (f_{cal}) given by Equation (2). The three J-O intensity parameters Ω_t ($t = 2, 4$, and 6) characterize the efficiency of interaction of the rare earth ion Ho^{3+} with the field PMN-PT ferroelectric crystal.

Step 4: The radiative transition probability $A(J', J)$, calculated radiative lifetimes τ_r and branching ratios β are obtained by Equations (12) to (14):

$$A(J', J) = A_{ed} + A_{md} = \frac{64\pi^4 e^2}{3h(2J+1)\lambda^3} (\chi_{ed} S_{ed} + \chi_{md} S_{md}) \quad (12)$$

$$\beta = \frac{A_{JJ'}}{\sum_{J'} A_{JJ'}} \quad (13)$$

$$\tau = \frac{1}{\sum_{J'} A_{JJ'}} \quad (14)$$

From Equations (1) to (11), the values of f_{cal} and f_{exp} , together with Ω_t ($t = 2, 4, 6$) of Ho^{3+} ion in the field environment of PMN-PT crystal, have been obtained. They are listed in Table 2. It can be found that the theoretical oscillator strength (f_{cal}) is consistent with the experiment oscillator strength f_{exp} . The root square deviation (δ_{rsm}) is 1.063×10^{-6} . It indicates that the obtained oscillator strengths are highly reliable. The obtained values of Judd–Ofelt intensity parameter are $\Omega_2 = 0.531 \times 10^{-20} \text{ cm}^2$, $\Omega_4 = 1.738 \times 10^{-20} \text{ cm}^2$, and $\Omega_6 = 0.530 \times 10^{-20} \text{ cm}^2$ for Ho^{3+} ion in PMN-32PT crystal.

Table 2. f_{cal} , f_{exp} , δ_{rsm} , and Ω_t ($t = 2, 4$, and 6) of PMN-32PT: $\text{Ho}^{3+}/\text{Yb}^{3+}$ crystal.

Transition	λ/nm	$f_{exp} \times 10^{-6}$	$f_{cal} \times 10^{-6}$	Ω_t ($t = 2, 4, 6$)/ cm^2
$^5\text{I}_8 \rightarrow ^5\text{F}_1 / ^5\text{G}_6$	451	14.2203	14.2234	
$^5\text{I}_8 \rightarrow ^5\text{F}_4 / ^5\text{S}_2$	541	6.9864	7.3646	$\Omega_2 = 0.531 \times 10^{-20}$
$^5\text{I}_8 \rightarrow ^5\text{F}_5$	643	5.4893	5.2341	$\Omega_4 = 1.738 \times 10^{-20}$
$^5\text{I}_8 \rightarrow ^5\text{I}_6$	1152	2.4753	1.0429	$\Omega_6 = 0.530 \times 10^{-20}$
$^5\text{I}_8 \rightarrow ^5\text{I}_7$	1943	2.2074	2.2074	
				$\delta_{rsm} = 1.063 \times 10^{-6}$

It is known that the spectroscopic quality factor is characterized by Ω_4/Ω_6 . In Table 3, the J-O intensity parameters Ω_t ($t = 2, 4$, and 6) and the spectroscopic quality factor Ω_4/Ω_6 for PMN-32PT: $\text{Ho}^{3+}/\text{Yb}^{3+}$ are compared with the values obtained for some laser crystals containing Ho^{3+} . The value of Ω_4/Ω_6 for Ho^{3+} in PMN-32PT crystal is 3.273, which is larger than that of laser crystals as well as $\text{LiNbO}_3:\text{In}^{3+}/\text{Ho}^{3+}$ [11], $\text{YAlO}_3:\text{Ho}^{3+}$ [12], $\text{YAG}:\text{Ho}^{3+}$ [13], and $\text{Gd}_3(\text{Al,Ga})_5\text{O}_{12}:\text{Ho}^{3+}/\text{Yb}^{3+}$ [14]. It is close to that of $\text{CNGG}:\text{Ho}^{3+}$ and $\text{GdScO}_3:\text{Ho}^{3+}$ crystals [16,17]. The high spectroscopic quality factor indicates the PMN-32PT: $\text{Ho}^{3+}/\text{Yb}^{3+}$ is a promising laser crystal.

Table 3. The values of Ω_t ($t = 2, 4$, and 6) $\times 10^{-20}/\text{cm}^2$ and Ω_4/Ω_6 of Ho^{3+} in laser crystals.

Crystal	Ω_2	Ω_4	Ω_6	Ω_4/Ω_6	Reference
$\text{LiNbO}_3:\text{In}/\text{Ho}$	1.069	13.575	10.076	1.347	[11]
$\text{YAlO}_3:\text{Ho}$	1.087	3.18	1.879	1.69	[12]
$\text{YAG}:\text{Ho}$	0.101	2.086	1.724	1.210	[13]
$\text{Gd}_3(\text{Al,Ga})_5\text{O}_{12}:\text{Ho}/\text{Yb}$	0.475	2.434	1.761	1.382	[14]
$\text{CNGG}:\text{Ho}$	2.85	2.35	0.76	3.09	[16]
$\text{GdScO}_3:\text{Ho}$	4.19	3.01	0.93	3.24	[17]
$\text{PMN-PT}:\text{Ho}/\text{Yb}$	0.531	1.738	0.530	3.273	This work

Table 4 lists the results of calculated electric and magnetic dipole spontaneous emission probabilities, radiative lifetimes, and branching ratios for the main emission transitions of Ho^{3+} in the field of PMN-32PT environment. It can be found from Table 4 that the transition probability $A(J' - J)$ of the ${}^5\text{F}_4/{}^5\text{S}_2 \rightarrow {}^5\text{I}_8$ (547 nm and 540 nm), ${}^5\text{F}_5 \rightarrow {}^5\text{I}_8$ (648 nm), and ${}^5\text{F}_4/{}^5\text{S}_2 \rightarrow {}^5\text{I}_7$ (741 nm and 755 nm) transitions is larger than that of other transitions. It can be predicted that there are three emissions which is consistent of an intense green, a red, and a weak NIR transition in the visible range. In addition, the radiative lifetime of ${}^5\text{I}_7$ energy level were calculated to be 5.45 ms, which is close to that of $\text{Gd}_3(\text{Al,Ga})_5\text{O}_{12}:\text{Ho}^{3+}/\text{Yb}^{3+}$ (${}^5\text{I}_7 \sim 5.87$ ms) crystal [14]. It is longer than that of $\text{LiNbO}_3:\text{In}^{3+}/\text{Ho}^{3+}$ (${}^5\text{I}_7 \sim 2.66$ ms) [11] and $\text{NaGd}(\text{MoO}_4)_2:\text{Ho}^{3+}/\text{Tm}^{3+}$ (${}^5\text{I}_7 \sim 4.02$ ms) laser crystals [20]. Table 5 lists the radiative lifetime of ${}^5\text{I}_7$, ${}^5\text{I}_6$, and ${}^5\text{I}_5$ of Ho^{3+} in different crystals for comparison. It can be seen that the radiative lifetime of Ho^{3+} in PMN-32PT crystal is shorter than that of $\text{MgWO}_4:\text{Ho}^{3+}$ crystal [21], but larger than those of other crystals reported in [11,20,22]. The longer radiative lifetime indicates that the energy storage capacity is high. It is in favor of achieving population inversion. Therefore, PMN-32PT crystal is suitable to be used as an up-conversion host material.

Table 4. The calculated results of the spectroscopic parameters of PMN-32PT: $\text{Ho}^{3+}/\text{Yb}^{3+}$ crystal.

Transitions	λ/nm	$ U^{(2)} ^2$	$ U^{(4)} ^2$	$ U^{(6)} ^2$	A_{ed}/s^{-1}	A_{md}/s^{-1}	A/s^{-1}	β	τ_{rad}/ms
${}^5\text{I}_7 \rightarrow {}^5\text{I}_8$	1986	0.0249	0.1344	1.5217	144	40	184	1.00	5.45
${}^5\text{I}_6 \rightarrow {}^5\text{I}_8$	1172	0.0083	0.0383	0.6918	336	0	336	0.84	2.51
$\rightarrow {}^5\text{I}_7$	2859	0.0319	0.1366	0.9308	39	23	62	0.16	
${}^5\text{I}_5 \rightarrow {}^5\text{I}_8$	902	0	0.0092	0.0936	133	0	133	0.41	3.09
$\rightarrow {}^5\text{I}_7$	1653	0.0027	0.0226	0.8887	165	0	165	0.51	
$\rightarrow {}^5\text{I}_6$	3920	0.0438	0.1705	0.5729	15	10	25	0.08	
${}^5\text{I}_4 \rightarrow {}^5\text{I}_8$	761	0	0	0.0077	17	0	17	0.09	5.36
$\rightarrow {}^5\text{I}_7$	1234	0	0.0033	0.1568	84	0	84	0.45	
$\rightarrow {}^5\text{I}_6$	2172	0.0022	0.0281	0.664	70	0	70	0.38	
$\rightarrow {}^5\text{I}_5$	4869	0.0312	0.1237	0.9099	11	4	15	0.08	
${}^5\text{F}_5 \rightarrow {}^5\text{I}_8$	648	0	0.4277	0.5686	5609	0	5609	0.78	
$\rightarrow {}^5\text{I}_7$	961	0.0177	0.3298	0.4340	1335	0	1335	0.19	0.14
$\rightarrow {}^5\text{I}_6$	1448	0.0102	0.1212	0.4995	231	0	231	0.03	
$\rightarrow {}^5\text{I}_5$	2297	0.0068	0.0271	0.1649	17	0	17	0.00	
$\rightarrow {}^5\text{I}_4$	4348	0.0001	0.0059	0.004	0	0	0	0.00	
${}^5\text{S}_2 \rightarrow {}^5\text{I}_8$	547	0	0	0.227	2360	0	2360	0.53	0.22
$\rightarrow {}^5\text{I}_7$	755	0	0	0.4096	1619	0	1619	0.36	
$\rightarrow {}^5\text{I}_6$	1027	0	0.0206	0.1541	349	0	349	0.08	
$\rightarrow {}^5\text{I}_5$	1391	0	0.0043	0.1062	76	0	76	0.02	
$\rightarrow {}^5\text{I}_4$	1947	0.0013	0.0279	0.2795	86	0	86	0.02	
$\rightarrow {}^5\text{F}_5$	3527	0	0.011	0.0036	2	0	2	0.00	
${}^5\text{F}_4 \rightarrow {}^5\text{I}_8$	540	0	0.2402	0.7079	9000	0	9000	0.75	
$\rightarrow {}^5\text{I}_7$	741	0	0.1988	0.0324	1589	0	1589	0.13	0.08
$\rightarrow {}^5\text{I}_6$	1000	0.0018	0.258	0.1697	960	0	960	0.08	
$\rightarrow {}^5\text{I}_5$	1343	0.0012	0.1314	0.4655	351	0	351	0.03	
$\rightarrow {}^5\text{I}_4$	1854	0.0001	0.0234	0.2587	50	0	50	0.00	
$\rightarrow {}^5\text{F}_5$	3233	0.1944	0.0923	0.008	14	8	22	0.00	

Table 5. The radiative lifetimes of Ho^{3+} in different crystal.

Crystals	${}^5\text{I}_7$	${}^5\text{I}_6$	${}^5\text{F}_5$	Reference
PMN-PT: $\text{Ho}^{3+}/\text{Yb}^{3+}$	5.45	2.51	0.14	This paper
$\text{MgWO}_4:\text{Ho}^{3+}$	6.18	2.98	0.21	[21]
$\text{GdYTaO}_4:\text{Ho}^{3+}$	5.33	2.35	0.12	[22]
$\text{NaGd}(\text{MoO}_4)_2:\text{Ho}^{3+}/\text{Tm}^{3+}$	4.02	2.46	0.15	[20]
$\text{LiNbO}_3:\text{Ho}^{3+}/\text{In}^{3+}$	2.66	1.32	0.09	[11]

3.6. Fluorescence Properties

The up-conversion emission spectra of PMN-32PT:Ho³⁺/Yb³⁺ crystals at 980 nm excitation are shown in Figure 7a. It consists of an intense green emission band at 553 nm, a red band at 663 nm, and a weak IR band at 755 nm. The three emission bands correspond to the ⁵F₄/⁵S₂→⁵I₈, ⁵F₅→⁵I₈, and ⁵F₄/⁵S₂→⁵I₇ transitions, respectively. This is consistent with the calculation results shown in Table 4 (the transition probability of ⁵F₄/⁵S₂→⁵I₈, ⁵F₅→⁵I₈, and ⁵F₄/⁵S₂→⁵I₇ are larger than that of other transitions).

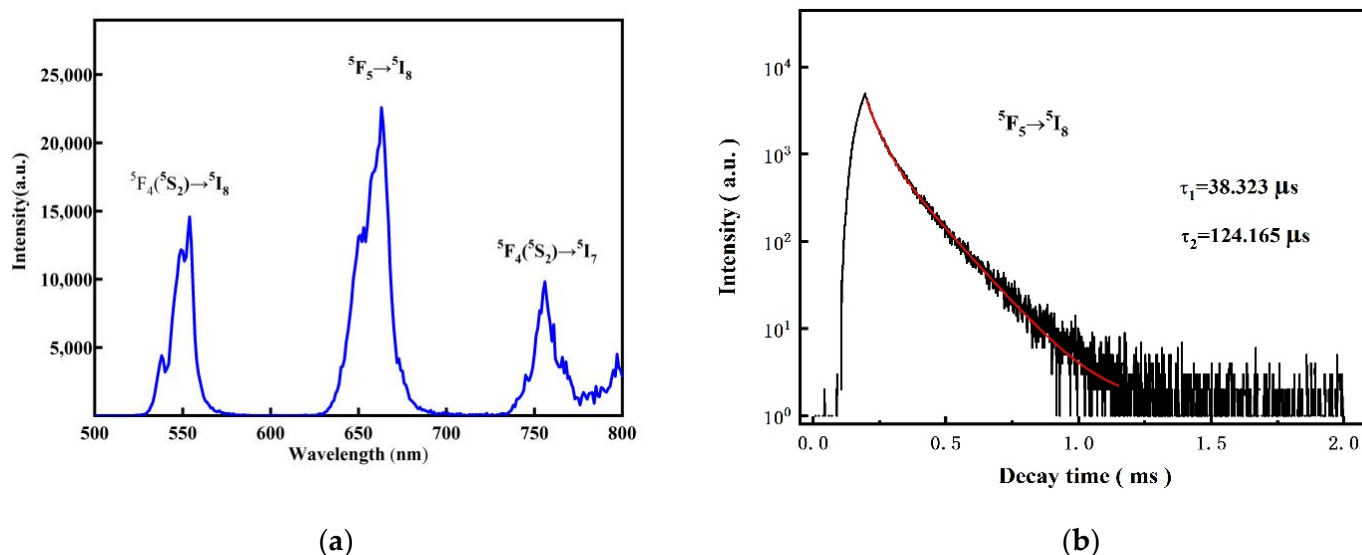


Figure 7. (a) UC emission spectra of PMN-32PT:Ho³⁺/Yb³⁺ crystals at 980 nm excitation. (b) Fluorescence decay curves of Ho³⁺ for ⁵F₅→⁵I₈ in PMN-32PT crystals at 980 nm excitation.

In addition, the fluorescence decay curves for ⁵F₅→⁵I₈ transitions of Ho³⁺ in PMN-32PT at 663 nm with the excitation of 980nm are shown in Figure 7b. The decay curves exhibited multi-exponential behavior, it can be well fitted with dual exponential function, fluorescence lifetime obtained by Equation (15):

$$\tau_f = (B_1\tau_1^2 + B_2\tau_2^2) / (B_1\tau_1 + B_2\tau_2) \quad (15)$$

where B_1 and B_2 are fitted parameters and τ_1 and τ_2 are measured decay lifetimes, the values of which are shown in Table 6.

Table 6. The measured B_1 , B_2 , τ_1 , and τ_2 of the fluorescence lifetime for PMN-32PT:Ho³⁺/Yb³⁺.

Transitions	λ (nm)	τ_1 (μ s)	τ_2 (μ s)	B_1	B_2	τ_f (μ s)
⁵ F ₅ → ⁵ I ₈	663	38.323	124.165	2971.481	1574.485	92.568

The fluorescence lifetime of ⁵F₅ level were fitting to be 92.568 μ s. Then, the quantum efficiency (η) obtained by Equation (16):

$$\eta = \tau_f / \tau_{rad} \quad (16)$$

The obtained quantum efficiency $\eta = 66\%$. Bigger quantum efficiency means more excited ions will deexcitation through laser transition emitting laser. It indicates that PMN-32PT:Ho³⁺/Yb³⁺ crystal is a promising luminescence material.

4. Conclusions

The new multifunctional crystal Ho³⁺/Yb³⁺ co-doped PMN-32PT is successfully grown using the flux method. Judd–Ofelt treatment has been performed on it for the first time. The

obtained J–O intensity parameters are $\Omega_2 = 0.531 \times 10^{-20} \text{ cm}^2$, $\Omega_4 = 1.738 \times 10^{-20} \text{ cm}^2$, and $\Omega_6 = 0.530 \times 10^{-20} \text{ cm}^2$. The radiative lifetime of ${}^5\text{I}_7$ is 5.45 ms. The measured fluorescence lifetime of ${}^5\text{F}_5 \rightarrow {}^5\text{I}_8$ is 92.568 μs at 980 nm excitation, the obtained quantum efficiency η of which is 66%. In addition, up-conversion luminescence emission bands, including an intense green emission band at 553 nm, a red band at 663 nm, and a weak infra-red band at 755 nm, are generated at the 980 nm excitation. The coercive field E_c of the as grown crystals PMN-32PT:Ho³⁺/Yb³⁺ is 11.86 kV/cm, which is nearly three times higher than that of PMN-32PT. These investigations show that the new multifunctional crystal PMN-32PT:Ho³⁺/Yb³⁺ possesses excellent ferroelectric and luminescence properties. It is a promising laser crystal and it has a potential application in innovative multifunctional devices.

Author Contributions: Conceptualization, J.Z. and Z.X.; methodology, J.Z.; software, X.W. and X.L.; validation, J.Z., X.W. and Z.X.; formal analysis, J.Z.; investigation, J.Z.; resources, X.W.; data curation, X.L. and S.G.; writing—original draft preparation, J.Z.; writing—review and editing, F.G.; visualization, X.W.; supervision, Z.X.; project administration, Z.X. and funding acquisition, Z.X. All authors have read and agreed to the published version of the manuscript.

Funding: This work was supported by the National Natural Science Foundation of China (Grant No. 51772235), the Key Laboratory of Optoelectronic Materials Chemistry and Physics, Chinese Academy of Sciences (Grant No.2016DP173016); Shaanxi Key Laboratory of Optoelectronic Functional Materials and Devices (Grant No.2015SZSJ-59-5, and No.20JS058), Fundamental Research Foundation of XATU of China (Grant No. XAGDXJJ16020).

Institutional Review Board Statement: Not applicable.

Informed Consent Statement: Not applicable.

Data Availability Statement: The data presented in this study are available on reasonable request from the corresponding author.

Conflicts of Interest: The authors declare no conflict of interest.

References

1. Lu, B.; Jian, X.; Lin, X.; Yao, Y.; Tao, T.; Liang, B.; Luo, H.; Lu, S. Enhanced electrocaloric effect in 0.73Pb(Mg_{1/3}Nb_{2/3})O₃-0.27PbTiO₃ single crystals via direct measurement. *Crystals* **2020**, *10*, 451. [CrossRef]
2. Tian, F.; Liu, Y.; Ma, R.; Li, F.; Xu, Z.; Yang, Y. Properties of PMN-PT single crystal piezoelectric material and its application in underwater acoustic transducer. *Appl. Acoust.* **2021**, *175*, 107827. [CrossRef]
3. Li, T.; Long, X.; Ye, M.; Wang, H.; Huang, H.; Zeng, X.; Ke, S. Growth and properties of (1-x)Pb(Zn_{1/3}Nb_{2/3})O₃-xPbTiO₃ (x = 0.07–0.11) ferroelectric single crystals by a top-seeded solution growth method. *Ceram. Int.* **2015**, *41*, 14427–14434. [CrossRef]
4. Liao, F.; Zhao, Y.; Chen, Z.; Zheng, Y.; Chen, H. Bridgman Growth and Photoelectric Property of Relaxor-Based Ferroelectric Single Crystal Pb(Sm_{1/2}Nb_{1/2})O₃-Pb(Mg_{1/3}Nb_{2/3})O₃-PbTiO₃. *Crystals* **2021**, *11*, 402. [CrossRef]
5. Li, F.; Matthew, J.; Bin, X.; Cheng, Z.; Elizabeth, C.; James, M.; Wang, J.; Luo, J.; Samuel, T.; Wesley, H.; et al. Giant piezoelectricity of Sm-doped Pb(Mg_{1/3}Nb_{2/3})O₃-PbTiO₃ single crystals. *Science* **2019**, *364*, 264–268. [CrossRef]
6. Xi, Z.; Han, A.; Fang, P.; Long, W.; Li, X.; Bu, Q. Structural and electrical properties of Ho³⁺-modified Pb(Zn_{1/3}Nb_{2/3})O₃-9PbTiO₃ single crystals. *J. Mater. Sci. Mater. Electron.* **2016**, *27*, 4223–4229. [CrossRef]
7. He, A.; Xi, Z.; Li, X.; Long, W.; Fang, P.; Zhao, J.; Yu, H.; Kong, Y. Optical properties of Ho³⁺ and Ho³⁺/Yb³⁺-modified PSN-PMN-PT crystals. *Mater. Lett.* **2018**, *219*, 64–67. [CrossRef]
8. Li, X.; Wang, Z.; He, C.; Liu, Y.; Long, X.; Han, S.; Pan, S. High piezoelectric response of a new ternary ferroelectric Pb(Ho_{1/2}Nb_{1/2})O₃-Pb(Mg_{1/3}Nb_{2/3})O₃-PbTiO₃ single crystal. *Mater Lett.* **2015**, *143*, 88–90. [CrossRef]
9. Yu, H. Growth and Characterization of Rare Earth Modified Ferroelectric Crystals. Master's Thesis, Xi'an Technological University, Xi'an, China, 2018.
10. Wang, H.; Yang, Q.; Sun, Y.; Jiang, X.; Huang, D. Optical spectroscopy studies of Ho/Yb co-doped yttrium lanthanum oxide transparent ceramics. *J. Lumin.* **2017**, *192*, 752–756. [CrossRef]
11. Dai, L.; Li, D.; Zhang, Y.; Qiang, Z.; Xu, C.; Xu, Y. Influence of In³⁺ ions concentration on spectroscopic properties of Ho:LiNbO₃ crystals. *J. Rare Earths.* **2012**, *30*, 780. [CrossRef]
12. Wang, R.; Huang, X.; Wang, Y.; Huang, R.; Zhang, P.; Zhu, S.; Yin, H.; Chen, Z.; Zheng, Y.; Zhou, G. Intense 3.9 μm emission of Ho³⁺ doped YAlO₃ single crystal. *Infrared Phys. Technol.* **2018**, *88*, 97–101. [CrossRef]
13. Brian, M.; Gary, W.; Norman, P. Energy levels and intensity parameters of Ho³⁺ ions in Y₃Al₅O₁₂ and Lu₃Al₅O₁₂. *J. Phys. Chem. Solids.* **2006**, *67*, 1567–1582.

14. Ryba-Romanowski, W.; Komar, J.; Niedzwiedzki, T.; Głowacki, M.; Berkowski, M. Excited state relaxation dynamics and up-conversion phenomena in $\text{Gd}_3(\text{Al,Ga})_5\text{O}_{12}$ single crystals co-doped with holmium and ytterbium. *J. Alloy. Compd.* **2016**, *656*, 573–580. [[CrossRef](#)]
15. He, C.; Tang, Y.; Zhao, X.; Xu, H.; Lin, D.; Luo, H.; Zhou, Z. Optical dispersion properties of tetragonal relaxor ferroelectric single crystals $0.65\text{Pb}(\text{Mg}_{1/3}\text{Nb}_{2/3})\text{O}_3-0.35\text{PbTiO}_3$. *Opt. Mater.* **2007**, *29*, 1055–1057. [[CrossRef](#)]
16. Zhou, Y.; Chen, J.; Dong, L.; Cao, S.; Zhang, Y.; Han, W.; Xu, H.; Liu, J. Growth and spectroscopic properties of Yb–Ho co-doped CNGG crystal. *Opt. Mater.* **2021**, *114*, 110998. [[CrossRef](#)]
17. Hu, D.; Dong, J.; Tian, J.; Wang, W.; Wang, Q.; Xue, Y.; Xu, X.; Xu, J. Crystal growth, spectral properties and Judd-Ofelt analysis of Ho: GdScO_3 crystal. *J. Lumin.* **2021**, *238*, 118243. [[CrossRef](#)]
18. Tan, X.; Xu, S.; Liu, F.; Wang, X.; Bernard, A.; Xiong, D.; Deng, W. Highly efficient up-conversion green emission in Ho/Yb co-doped yttria-stabilized zirconia single crystals. *J. Lumin.* **2019**, *209*, 95–101. [[CrossRef](#)]
19. Zhang, P.; Zhang, L.; Hong, J.; Wang, Y.; Chen, G.; Chen, Z.; Wang, X.; Shi, C.; Hang, Y. Spectroscopic properties of Ho^{3+} -doped PbF_2 single crystal for 2 lm lasers. *Opt. Mater.* **2015**, *46*, 389–392. [[CrossRef](#)]
20. Wang, C.; Yin, H.; Li, A.; Wu, Y.; Zhu, S.; Chen, Z.; Zhang, G.; Su, K. Growth, thermal and spectral properties of Tm^{3+} , Ho^{3+} co-doped $\text{NaGd}(\text{MoO}_4)_2$ Crystal[J]. *J. Alloy. Compd.* **2014**, *615*, 482–487. [[CrossRef](#)]
21. Zhang, L.; Pavel, L.; Josep, M.; Esrom, K.; Lin, H.; Zhang, G.; Elena, V.; Elena, D.; Alexey, K.; Liudmila, F. Growth, spectroscopy and first laser operation of monoclinic $\text{Ho}^{3+}:\text{MgWO}_4$ crystal. *J. Lumin.* **2019**, *213*, 316–325. [[CrossRef](#)]
22. Dou, R.; Liu, W.; Zhang, Q.; Peng, F.; Sun, G.; Luo, J.; Chen, Y.; Sun, D. Growth and spectroscopic properties of Ho^{3+} doped GdYTaO_4 single crystal. *J. Lumin.* **2018**, *10*, 096. [[CrossRef](#)]